VIROLOGY

Single-cell herpes simplex virus type 1 infection of neurons using drop-based microfluidics reveals heterogeneous replication kinetics

Jacob P. Fredrikson[1,2]†, Luke F. Domanico[3]†, Shawna L. Pratt[1,2], Emma K. Loveday[1,2], Matthew P. Taylor[3]*, Connie B. Chang[1,2,4]*

Single-cell analyses of viral infections reveal heterogeneity that is not detected by traditional population-level studies. This study applies drop-based microfluidics to investigate the dynamics of herpes simplex virus type 1 (HSV-1) infection of neurons at the single-cell level. We used micrometer-scale Matrigel beads, termed microgels, to culture individual murine superior cervical ganglia (SCG) neurons or epithelial cells. Microgel-cultured cells are encapsulated in individual media-in-oil droplets with a dual–fluorescent reporter HSV-1, enabling real-time observation of viral gene expression and replication. Infection within drops revealed that the kinetics of initial viral gene expression and replication were dependent on the inoculating dose. Notably, increasing inoculating doses led to earlier onset of viral gene expression and more frequent productive viral replication. These observations provide crucial insights into the complexity of HSV-1 infection in neurons and emphasize the importance of studying single-cell outcomes of viral infection. These techniques for cell culture and infection in drops provide a foundation for future virology and neurobiology investigations.

INTRODUCTION

Single-cell analyses have advanced our understanding of cellular physiology and viral infection by facilitating the observation of underrepresented cellular and viral phenotypes. In vitro studies of viral infection traditionally rely on population-level approaches where cells are cultured and infected in well plates (1). However, these approaches often overlook the heterogeneous dynamics of viral infection, obscured by productive viral replication (1–5). Single-cell methods for both culture and infection provide increased insights into infectious virus production, viral replication kinetics, and genetic variability (4–11).

Herpes simplex virus type 1 (HSV-1) is a ubiquitous pathogen, which infects neurons to establish lifelong persistent and recurrent disease (12, 13). The replication, persistence, and transmission of HSV-1 are determined by the regulation and temporal expression of viral genes (14, 15). Single-cell studies of HSV-1 infection in epithelial cells have revealed variability in the dynamics of viral replication (2, 16, 17). In addition, single-cell transcriptional analysis of HSV-1–infected epithelial cells observed a highly variable abundance of viral transcripts temporally classified as immediate-early, early, and late genes. While our understanding of infection through single-cell analysis is improving, single-cell HSV-1 infection of isolated neurons has not been achieved to date.

A powerful technique for studying single-cell viral infection is drop-based microfluidics (1, 3, 18, 19). This method generates emulsions containing monodisperse, picoliter-sized, aqueous drops suspended in oil that can be used in various single-cell assays. Drop-based microfluidic methods facilitate the encapsulation of millions of single cells, enabling in-depth, high-throughput analysis of viral and cellular heterogeneity (1, 3, 18). However, these methods have previously focused on infections in nonadherent cells (18) that were suspended in aqueous drops (20–26). Neurons require a soft, viscoelastic solid substrate that supports neurite development and growth, which is not compatible with the aqueous environment produced using drop-based microfluidics (27). Extending drop-based capabilities for adherent cultures at the single-cell level would greatly facilitate understanding of viral infection in physiologically relevant cells. Support for the growth and development of cells that require solid substrates can be achieved with microscale hydrogel beads, referred to as microgels (28, 29). Microgels provide a homogeneous and highly tunable biomimetic growth environment and have been previously used to culture multiple cell types such as neurospheres, embryonic stem cells, and induced pluripotent stem cell aggregates (28, 29). While microgels can offer a foundation for neuronal growth and maturation, their application in drop-based methodologies for viral infections has never been assessed. Single-cell evaluation of population-level HSV-1 infection of neurons has provided valuable knowledge (16), but methods supporting the infection and analysis of isolated neurons remain limited. Therefore, the development of innovative techniques for individual neuron culture would facilitate single-cell studies of HSV-1 infection.

In our study, we use drop-based microfluidics to culture, inoculate, and observe live-cell tracking of HSV-1 infection across different cell types, including individual murine superior cervical ganglia (SCG) neurons and Vero cells. The single cells are embedded in Matrigel microgels and subsequently encapsulated in drops containing defined inoculating doses of HSV-1. HSV-1 infection is visualized using a recombinant fluorescent protein–expressing reporter virus. Our results demonstrate that cells cultured within microgels are not accessible to infection, whereas cells located on the microgel surface support a greater extent of infection compared to suspension cells. In addition, the onset of viral gene expression and replication kinetics were monitored, revealing that higher inoculating doses result in an

[1]Department of Chemical and Biological Engineering, Montana State University, P.O. Box 173920, Bozeman, MT 59717, USA. [2]Center for Biofilm Engineering, Montana State University, 366 Barnard Hall, Bozeman, MT 59717, USA. [3]Department of Microbiology and Cell Biology, Montana State University, P.O. Box 173520, Bozeman, MT 59717, USA. [4]Department of Physiology and Biomedical Engineering, Mayo Clinic, 200 First St. SW, Rochester, MN 55905, USA.
*Corresponding author. Email: mptaylor@montana.edu (M.P.T.); chang.connie@mayo.edu (C.B.C.)
†These authors contributed equally to this work.

earlier onset and progression of viral replication. In conclusion, these findings demonstrate that microgels provide a solid surface that supports neuronal growth and development, enabling productive single-cell HSV-1 infection within drops. The use of microgels for high-throughput single-cell culturing can provide a valuable tool for future research in neurobiology and virology studies, further enhancing our understanding of factors that affect viral replication dynamics.

RESULTS

We developed drop-based microfluidic approaches to investigate the dynamics of HSV-1 infection in individual primary neurons (Fig. 1). First, individual murine embryonic SCG neurons are suspended in a Matrigel precursor solution that is processed into microgels with diameters of approximately 100 μm using a microfluidic device (Fig. 1A). The density of cells in the Matrigel solution will produce one cell in every 10 microgels on average, following Poisson loading statistics, to minimize the number of microgels with multiple cells. The microgel-embedded neurons are cultured for 1 week to allow for the growth and development of neurite extensions. Subsequently, neurons are infected using a co-flow inoculation device, where hydrogels and virus are simultaneously emulsified into drops. Co-flow inoculation allows precise control of the viral inoculating dose to

Fig. 1. Experimental schematic for the embedding, growth, and infection of individual neurons within microfluidic drops. (**A**) SCG neurons are suspended in liquid Matrigel and emulsified in oil. The drops are incubated at 37°C for 35 min for gelation. The microgels and neurons are washed and placed in media for 7 days for neuronal maturation. (**B**) After 7 days, the neurons are co-flowed with viral inoculum and emulsified in fluorinated oil. (**C**) A dual-fluorescent HSV-1 recombinant is used to visualize infection. Initiation of viral gene expression is reported by YFP detection. Late gene expression is reported by RFP detection. (**D**) Individual cells can be tracked over time to observe the progression of FP detection.

achieve single-cell infection (Fig. 1B). To visualize infection dynamics and replication kinetics, cells were infected with a dual–fluorescent protein (FP)–expressing reporter HSV-1. This dual-reporter HSV-1 expresses enhanced yellow fluorescent protein (eYFP) driven by an immediate-early human cytomegalovirus (*CMV*) promoter and an mCherry-VP26 fusion driven by the endogenous late promoter (*30*). Detection of virus-expressed YFP reports the onset of viral gene expression upon infection, while the detection of mCherry [red fluorescent protein (RFP)] corresponds to late viral gene expression and virion assembly (Fig. 1C). To observe infection dynamics at the single-cell level, we immobilized drops on a "DropSOAC" microfluidic device that enables incubation and fluorescence microscopy over the course of infection (Fig. 1D) (*31*, *32*). The DropSOAC allows us to monitor and analyze the progression of HSV-1 infection in individual neurons over time.

Single-cell infection outcomes of Vero cells with dual-reporter HSV-1

To investigate the interactions between cells, microgels, and viral inoculum, we first conducted a study focusing on HSV-1 infection of Vero cells and microgels. Vero cells are an epithelial cell line commonly used for studying HSV-1 infections in vitro (*12*). We first evaluated whether the location of the cell in the microgel alters the likelihood of a cell becoming infected. Vero cells were grown either "in microgels" or "on microgels" before being inoculated at 10 plaque-forming units (PFU) per drop using a co-flow microfluidic device (Fig. 2A). YFP detection was used to evaluate the percentage of infected cells (*30*). For the in-microgel condition, Vero cells were first embedded within 100-μm microgels before emulsification with viral inoculum in drops. In-microgel infections produce only $1.7 \pm 1.4\%$ YFP-positive detection at 16 hours post-infection (hpi) (Fig. 2, B, C, and F). The location of the cell in the microgel is a random event from the drop-making process, with a low percentage of cells located on the periphery of the microgel. No cells enclosed within the microgel expressed YFP (Fig. 2B). The cells that did express YFP were all found at the edge of the microgel (Fig. 2C). For the on-microgel condition, Vero cells were seeded onto prefabricated microgels and allowed to adhere for 4 hours before inoculation in drops. On-microgel infections produce $76.8 \pm 5.0\%$ YFP-positive detection at 16 hpi (Fig. 2, D and F). We compared our microgel-based methodology with previous microfluidic approaches for infection in drops, excluding microgels (*21*, *25*). In our experiments, Vero cells were emulsified in drops suspended in media with viral inoculum, creating an "in-suspension" condition. Under these in-suspension infection conditions, we observed a $50.0 \pm 3.7\%$ YFP-positive detection at 16 hpi (Fig. 2, E and F). The reduced extent of YFP-positive cells could be attributed to decreased cellular viability. Thus, to evaluate Vero cell viability, uninfected cells were suspended in drops without the virus and incubated for 16 hours. Drops were then broken at 0 and 16 hours of incubation, and the collected cells were stained with CellTracker CMFDA to identify metabolically active cells and propidium iodide (PI) for staining the nuclei of dead cells. Our analysis revealed a cellular viability of $99 \pm 1.0\%$ after 0 hours and $92 \pm 1.8\%$ after 16 hours of incubation, based on fluorescent staining (fig. S1). Despite a statistically significant difference in viability between the two time points, it does not explain the reduced infectivity of Vero cells in suspension. Consequently, we speculate that Vero cells in suspension remain viable but may be potentially less accessible or permissive to HSV-1 infection compared to the same cells cultured on microgels.
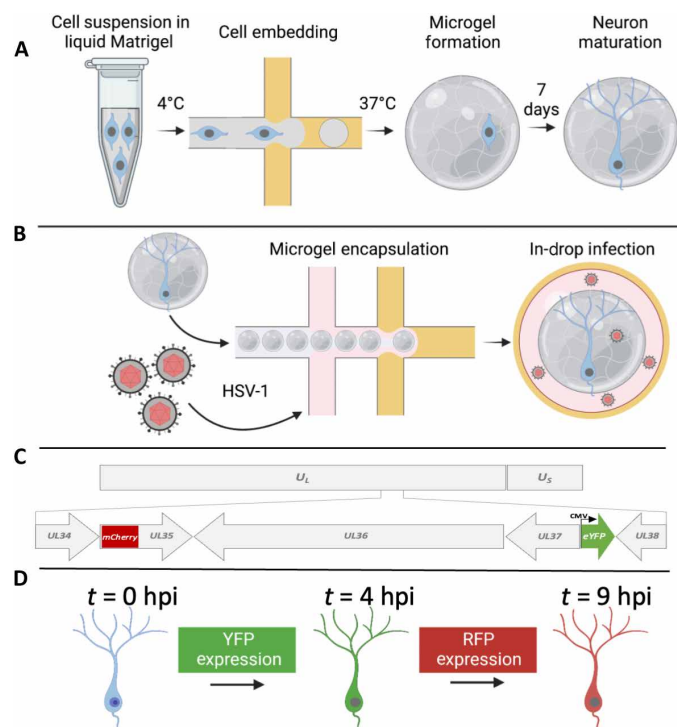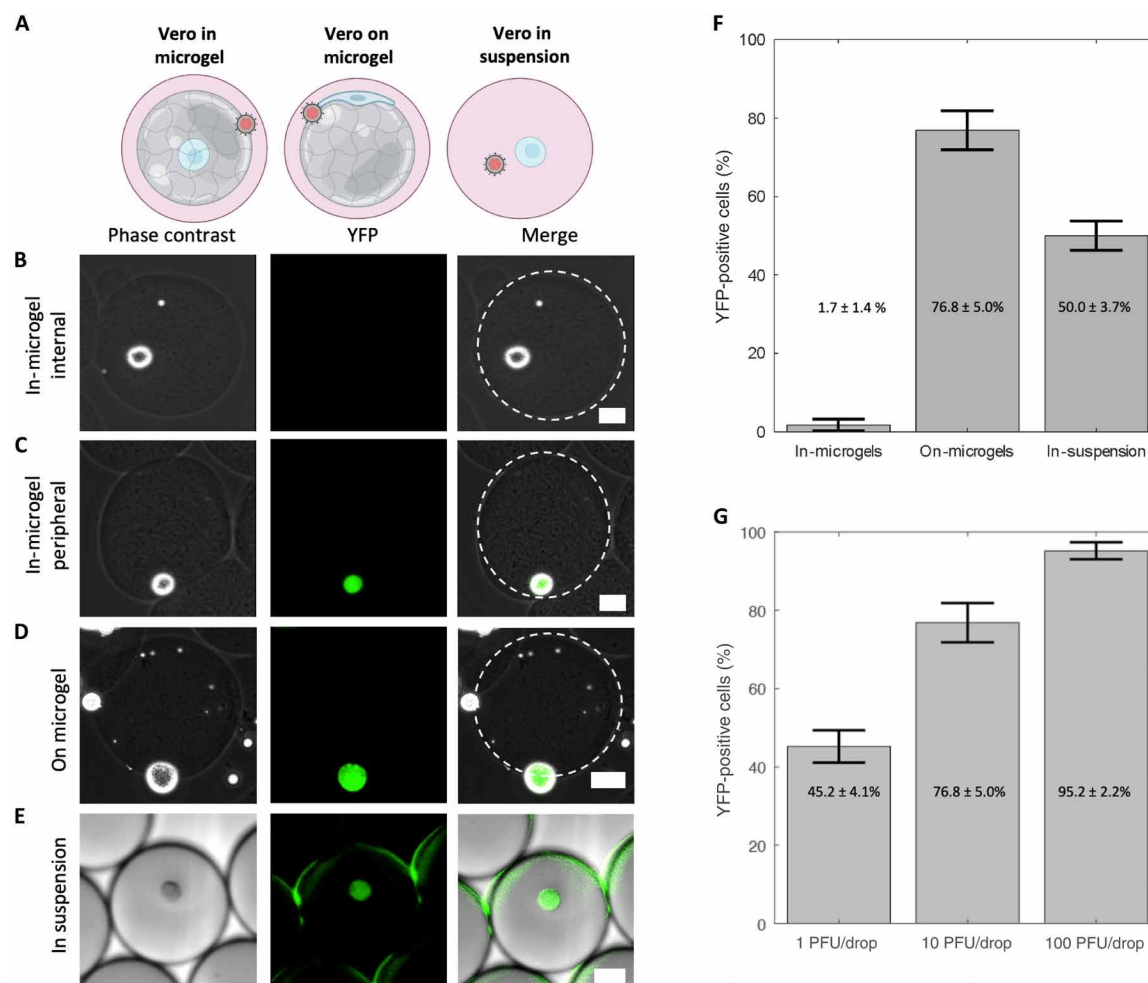
Fig. 2. Impacts of microgels on infection. (**A**) Model of Vero cell culture in microgels, on microgels, or in suspension for co-flow inoculation. (**B** to **E**) Representative phase contrast, YFP, and merged images of infected cells. Scale bars, 25 μm. (B) In microgels with an internally positioned cell. (C) In microgels with a peripherally positioned cell. (D) On microgel. (E) In suspension. (**F**) Bar graphs showing the percentage of YFP-positive cells. Vero cells cultured as indicated and co-flow inoculated with 10 PFU per drop of dual-reporter HSV-1. (**G**) Bar graphs showing the percentage of YFP-positive cells from Vero cells cultured on microgels inoculated with 1, 10, and 100 PFU per drop. This trend was statistically significant (one-way ANOVA, $P = 1.3 \times 10^{-5}$). All infections in (F) and (G) were performed in triplicate with an average number of 200 cells per condition per replicate. Error bars show SDs.

Once we determined that Vero cells grown on microgels were the most susceptible to infection, we further evaluated the effect of infectious dose with the co-flow inoculation system. Cells on microgels were inoculated with doses ranging from 1, 10, and 100 PFU per drop. As inoculating dose increased, the percentage of YFP-positive cells increased from $45.2 \pm 4.1\%$ at 1 PFU per drop to $76.8 \pm 5.0\%$ at 10 PFU per drop and $95.2 \pm 2.2\%$ at 100 PFU per drop (Fig. 2G). The extent of YFP-positive cells with increasing inoculating dose was statistically significant [one-way analysis of variance (ANOVA), $P = 1.3 \times 10^{-5}$, df = 8]. This observation is consistent with the expectation that increasing inoculating dose leads to greater extents of infection (33).

We hypothesized that the low number of Vero cells embedded in microgels with detectable YFP is due to the inability of virions to penetrate Matrigel (34, 35). While Matrigel is a porous material, the pore size is approximately 150 nm, nearly the same size as the 150- to 250-nm-diameter HSV-1 virion (36). To test our hypothesis that virion diffusion through Matrigel is limited, the interaction between mCherry-VP26–labeled virions and Matrigel was observed on a confocal microscope. Matrigel was pipetted onto glass and allowed to gel into a disc before the addition of mCherry-VP26–labeled virions and subsequent imaging. Over 1.5 hours, we observed that no HSV-1 virions diffuse past the interface of a Matrigel disc (Fig. 3). In addition, we saw no accumulation of virions at the interface, indicating that the HSV-1 particles were not adhering to or penetrating the gel and becoming immobilized (Fig. 3A). These data demonstrate that HSV-1 virions likely do not diffuse through the Matrigel. To assess whether the lack of particle diffusion is related to size, we also evaluated the diffusion of fluorescent nanoparticles with average diameters of 160 nm. Like the fluorescent virions, fluorescent nanoparticles do not enter the Matrigel but do accumulate at the aqueous interface (Fig. 3B). These observations suggest that only cells that are located on the surface of Matrigel microgels are accessible to HSV-1 infection.
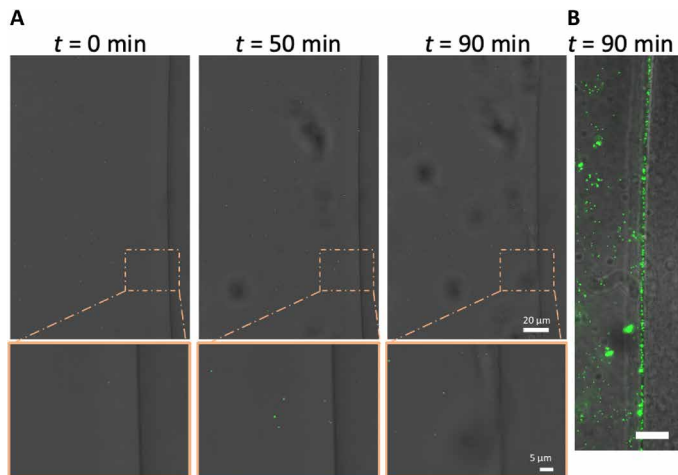
Fig. 3. HSV-1 virions cannot enter Matrigel. (**A**) Representative images of time-lapse confocal microscopy of mRFP-labeled HSV-1 virions diffusing next to a disc of Matrigel (right side of image). Images were acquired every 10 min for 90 min in bright field and mRFP (false-colored green). (**B**) Nanoparticles (green) were added to the solution surrounding the Matrigel disc. Scale bar, 15 μm; t = 60 min.

The initial evaluations of Vero cell infections demonstrate that microgels provide a scaffold that can be used to culture and infect adherent cell lines in drop-based assays. In comparison to embedded cells, Vero cells cultured on the microgel have increased accessibility to HSV-1 infection and yield the highest percentage of detected infection. Cells that were not located on the surface of the microgels were unlikely to become infected with HSV-1 as the virions do not diffuse through Matrigel. The reduced infection observed in suspended Vero cells is hypothesized to be caused by changes to cellular permissiveness to HSV-1 infection.

Growth of individual SCG neurons in microgels

We next used our microgel culturing system for the in vitro growth and development of individual primary mouse SCG neurons. Dissociated SCG neurons, unlike adherent epithelial cells such as Vero cells, require structural support to promote neurite development during both culture and microfluidic manipulation. Neurites, including axons and dendrites, are critical for neuronal homeostasis, metabolic regulation, and synaptic signaling (*27*, *37*). To foster neurite development, SCG neurons were embedded in Matrigel microgels using a drop-based microfluidic device. Subsequently, the neurons were cultured to allow maturation and neurite extension over a period of 7 days. After 7 days in culture, the neuronal cell bodies migrated to the peripheral regions of the microgels, and robust neurites were observed either within the microgels or on their external curvature (Fig. 4A). To confirm that the embedded neurons reached physiological maturity, we performed immunofluorescence staining for phosphorylated neurofilament H (N-F), a protein localized in axons of mature neurons. SCG neurons grown in Matrigel microgels exhibited visible N-F immunostain in neurite extensions (Fig. 4B, red). These findings indicate that microgels provide a suitable growth environment for individual neurons, enabling the production of neurite extensions and promoting maturation.

Single-cell infection of SCG neurons

We next investigated the capacity to infect individual mature SCG neurons within microgels using dual-reporter HSV-1. Microgel-cultured neurons were infected with different inoculating doses of 1, 10, or 100 PFU per drop and imaged for YFP at 16 hpi. A representative image of YFP expression in an infected neuron is shown in Fig. 4D. At the lowest viral concentration of 1 PFU per drop, $37.3 \pm 6.3\%$ of SCG neurons exhibited detectable YFP (Fig. 4C). SCG neurons infected with 10 and 100 PFU per drop demonstrated significantly higher percentages of infection, with $61.6 \pm 2.5\%$ and $72.2 \pm 6.6\%$ of YFP-positive cells, respectively (Fig. 4C). To determine the relationship between inoculating dose and YFP positivity, we conducted a one-way ANOVA and found that inoculating dose had a significant impact on YFP detection across 1, 10, and 100 PFU per drop inoculations ($P = 5.9 \times 10^{-4}$, df = 8). Our results demonstrate that primary SCG neurons cultured in microgels and infected in microfluidic drops are susceptible to HSV-1 infection and support viral gene expression, as reported by YFP detection.

Timing and outcomes of viral gene expression in individual SCG neurons

We next examined the kinetics of viral gene expression in single neurons by detecting YFP for the onset of viral gene expression and RFP onset for late viral gene expression (*30*). To monitor and quantify the timing of viral gene expression in single neurons infected with dual-reporter HSV-1, mature microgel-cultured neurons were emulsified with viral inoculum and placed in a microfluidic chamber called a DropSOAC (Fig. 5A). The DropSOAC immobilizes the drops and allows for temporal tracking and fluorescence quantification of individual cells (*31*). Images of infected neurons were acquired every 15 min for 16 hours, with image acquisition starting 1 hour after in-drop inoculation (Fig. 5B and movie S1). The onset of FP detection was determined by the point at which the fluorescent pixel intensity surpassed the background threshold value (Fig. 5C).

To assess the impact of inoculating dose on the detection of HSV-1–expressed FPs in single neurons, microgel-cultured neurons were infected with 1, 10, and 100 PFU per drop and imaged for 16 hours. Neurons infected with 1 PFU per drop exhibited an onset of YFP detection at 4.9 ± 2.0 hpi (Fig. 5D). Neurons infected with 10 PFU per drop exhibited an onset of YFP detection at 5.5 ± 2.8 hpi. Neurons infected with 100 PFU per drop displayed the earliest onset of YFP detection at 3.3 ± 1.7 hpi. On the basis of a one-way ANOVA, we found that the timing of YFP detection decreased with increased inoculating dose ($P = 1.1 \times 10^{-7}$, df = 166), indicating that the inoculating dose significantly affects the onset of HSV-1 gene expression in single neurons.

Neurons were further examined for RFP detection, which correlates with the progression of viral replication. We observed that only 2.6 and 6.5% of YFP-positive cells become RFP positive at 1 and 10 PFU per drop, respectively (Fig. 5D). However, neurons infected with 100 PFU per drop exhibited much higher rates of RFP positivity, with 55.7% of YFP-positive cells becoming RFP positive by 16 hpi (Fig. 5D). The average timing of RFP detection in cells infected with 100 PFU per drop was 9.4 ± 2.5 hpi (Fig. 5D). No cells were detected that were RFP positive and not YFP positive. These data demonstrate that in our single-neuron drop-based culturing and infection system, we can observe dose-dependent progression of HSV-1 infection in real time.
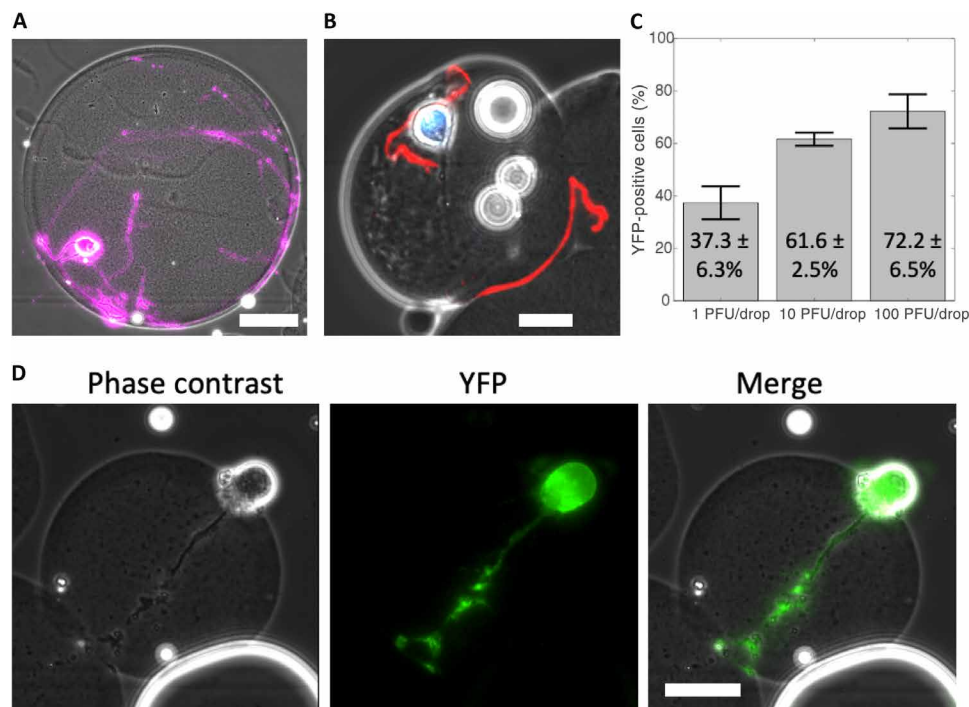
Fig. 4. Microgels support neuronal maturation and infection. (**A**) Representative image of a mature SCG neuron in a Matrigel microgel after 7 days in culture. Cells were stained with calcein AM, false-colored purple. Scale bar, 25 μm. (**B**) Mature SCG neuron grown in a microgel immunostained for phosphorylated neurofilament H (red) and nuclei (blue). Scale bar, 25 μm. (**C**) Bar graph showing the percentage of YFP-positive neurons following infection at 1, 10, and 100 PFU per drop. Infections were performed in triplicate with an average of 158 cells per replicate per condition. Statistical significance evaluated by one-way ANOVA ($P = 5.9 \times 10^{-4}$). Error bars show SD. (**D**) Representative phase contrast, YFP, and merged images of an infected SCG neuron. Scale bar, 25 μm.

From the time-lapse data, we estimated the progression of viral replication by calculating the timing between YFP and RFP detection in each infected neuron. At 100 PFU per drop, we observed an average time of 6.6 ± 2.2 hours between YFP and RFP detection (Fig. 5E). To determine whether the timing of YFP detection influences the timing of RFP detection, we implemented a linear regression model, which predicts that single neurons will become detectably RFP positive 6.6 ± 1.8 hours after onset of YFP detection [$t_{RFP+} = 6.6 (\pm1.8) + 1.0 (\pm0.6)t_{YFP+}$, $P = 0.002$]. However, the correlation between the onset of YFP detection and conversion to YFP/RFP-positive detection was weak ($R^2 = 0.23$), indicative of the heterogeneous infection in single neurons. Thus, we conclude that the timing of YFP detection is not predictive of the timing of RFP detection.

We also monitored and quantified the timing of FP detection in Vero cells infected with dual-reporter HSV-1. Similar to our previous on-microgel condition, Vero cells were cultured on microgels, then encapsulated with viral inoculum, and placed in a DropSOAC device. We observed similar trends in single Vero cells to those observed in single neurons (Fig. 6A). Vero cells infected with 1 PFU per drop exhibited an onset of YFP detection at 6.6 ± 2.6 hpi. Vero cells infected with 10 PFU per drop exhibited an onset of YFP detection at 5.0 ± 2.0 hpi. Vero cells infected with 100 PFU per drop displayed the earliest onset of YFP detection, at 3.5 ± 1.5 hpi. Using a one-way ANOVA, we found that the timing of YFP detection decreased with increasing inoculating doses in single Vero cells ($P = 1.9 \times 10^{-35}$, df = 649) (Fig. 6A).

In a similar trend to neuronal infection, 1.9 and 4.6% of YFP-positive Vero cells became RFP positive at 1 and 10 PFU per drop, while 64.2% of YFP-positive Vero cells became RFP positive at 100 PFU per drop (Fig. 6, A to C). From the time-lapse data, linear regression predicts that at 100 PFU per drop, Vero cells become detectably RFP positive 6.4 ± 1.0 hours after onset of YFP detection; however, the fit is weak [linear regression, $t_{RFP+} = 6.4 (\pm1.0) + 0.9 (\pm0.3) t_{YFP+}$, $P = 1.1 \times 10^{-7}$, $R^2 = 0.22$] (Fig. 6B). The concordance of both the extent of RFP-positive cells and the progression of YFP-to-RFP detection suggests that inoculating dose, not cell type, plays an important role in determining outcomes of HSV-1 infection.

In summary, we demonstrate the use of microfluidic methods for the culture and infection of Vero cells and primary SCG neurons to observe progression of HSV-1 infection with single-cell resolution. We find that inoculating dose influences the extent and frequency of progression for HSV-1 infection in both cell types. Specifically, at higher inoculating doses, cells express detectable YFP earlier and are more likely to progress to detectable RFP progression and viral replication. These experiments validate the use of drop-based culturing and live-cell tracking of HSV-1 across different cell types susceptible to HSV-1 infection.

DISCUSSION

In this study, we used drop-based microfluidics for the culturing of individual cells and the subsequent infection with HSV-1. Culturing cells using Matrigel microgels enabled both neurons and adherent
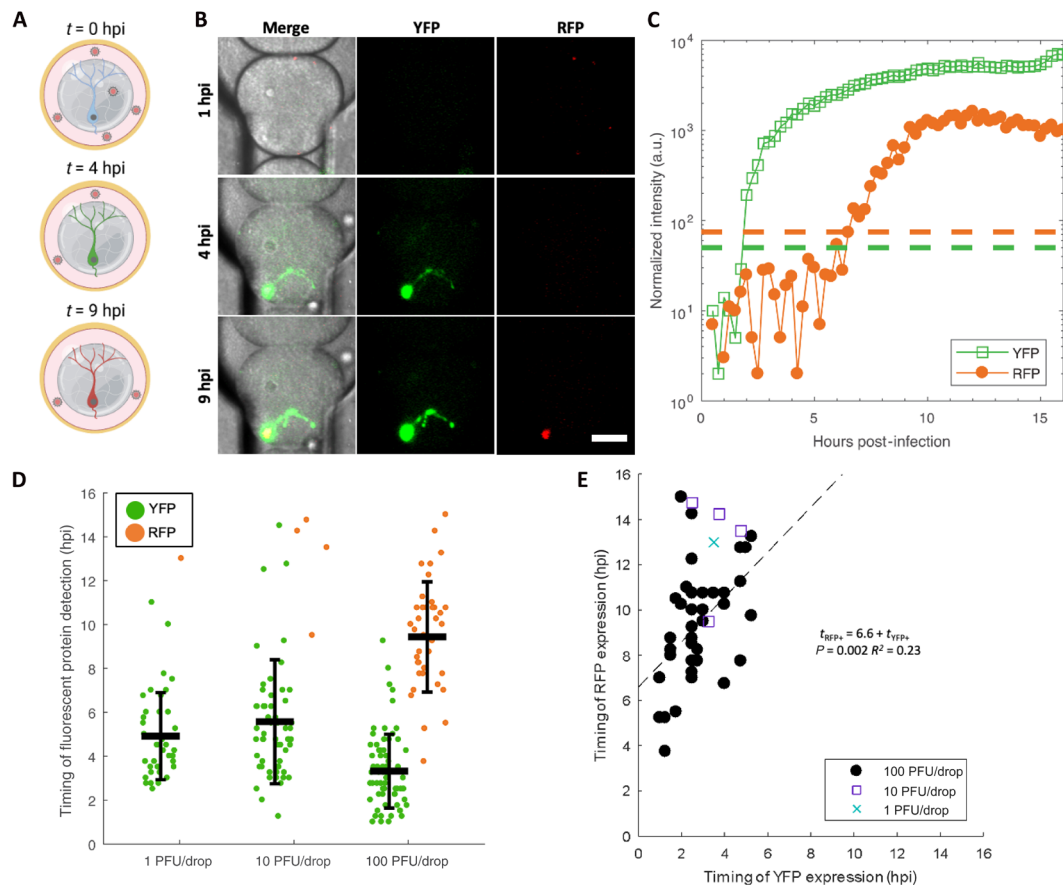
Fig. 5. The effect of inoculating dose on neuronal infection progression and kinetics. (**A**) Schematic of experimental design for temporal tracking of YFP and RFP. (**B**) Representative images from time-lapse microscopy of an infected neuron expressing YFP and RFP in a DropSOAC chamber (*31*). Scale bar, 50 μm. (**C**) Normalized intensities of YFP (open green squares) and RFP (filled red circles) for the representative cell in (B). Dashed lines represent the threshold value above which cells are considered positive for FP detection. (**D**) Timing of YFP and RFP detection plotted with the mean and SD. Each data point represents quantitation from single neurons. Statistical significance was evaluated by one-way ANOVA ($P = 1.1 \times 10^{-7}$). Error bars show SD. Infections were performed three to four times and pooled together for analysis with a total of 174 cells analyzed. (**E**) Correlation of YFP versus RFP detection time for RFP-positive neurons (1 PFU per drop, blue X; 10 PFU per drop, purple square; 100 PFU per drop, black circle). A linear regression fit to evaluate the significance of correlation is plotted as a dashed line with the fit.

epithelial cells to maintain physiologically relevant morphologies. Following the culturing of cells within these microgels, we implemented a co-flow inoculation approach that allows for precise control over infection conditions. Subsequently, a specialized microfluidic DropSOAC device (*32*) enabled the immobilization of individually infected cells and real-time observation of HSV-1 replication through detection of virally expressed FPs. Collectively, these techniques offer innovative means to culture and study isolated cells and observe real-time HSV-1 replication kinetics at the single-cell level.

Neurons are the focal point of HSV-1 persistence, morbidity, and mortality; therefore, it is important to understand how HSV-1 infection progresses in primary neurons (*12*). However, primary neurons require a solid substrate that supports neurite development and growth, limiting their usability in an aqueous drop environment. To produce a solid substrate for cells, we embedded primary SCG neurons in Matrigel microgels, which promoted their maturation and facilitated microfluidic manipulation. We observed that microgel-cultured SCG neurons grew robust neurite extensions that follow the external curvature of the microgels. In addition, immunofluorescence imaging demonstrated the presence of phosphorylated neurofilament

H in the neurite extensions, indicating SCG neuron maturation and axonal development, which was achieved by 7 days in culture. The use of Matrigel provided not only the solid substrate but also laminin cofactors that are important for SCG survival and development (*38*, *39*). This work shows that Matrigel microgels provide the necessary growth factors and support for sustained growth and viability of neurons in culture.

Microgels provide support for subsequent microfluidic manipulation of cultured neurons for in-drop infection. We achieved $72.2 \pm 6.6\%$ infection of individual neurons grown in microgels. Infections elicited a wide distribution of YFP detection onset in single neurons, ranging from 1.25 to 16 hpi. The variability could be the result of HSV-1 entry at distal axon sites leading to delays in replication. Yet, it is more likely the result of a heterogeneous establishment of infection, as a wide distribution of YFP detection onset also occurred in Vero cells. Similarly, we observed large differences in the time it takes a YFP-positive cell to progress to RFP positivity in both cell types. On the basis of these observations, we hypothesize that the establishment and progression of HSV-1 infection is heterogeneous across individual neurons. This hypothesis is supported by recent
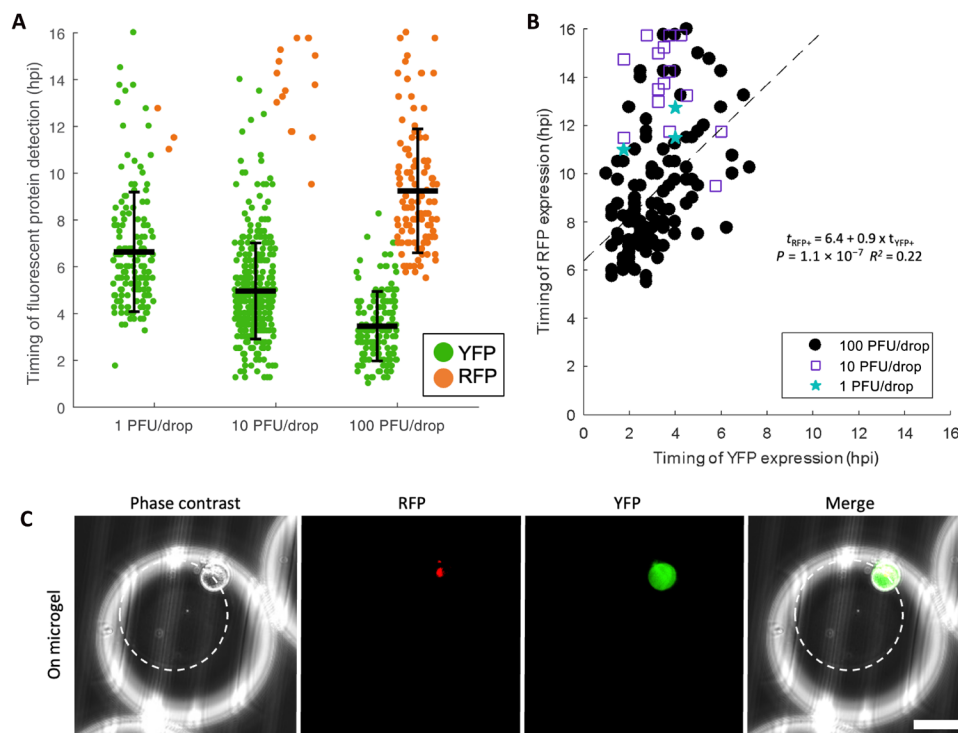
Fig. 6. HSV-1 replication kinetics in Vero cells. (A) Timing of YFP and RFP expression in individual Vero cells plotted with the mean and SD. Timing of YFP detection decreased with increased inoculating dose (one-way ANOVA, $P = 1.9 \times 10^{-35}$). Error bars show SD. Infections were performed three times and pooled together for analysis with a total of 669 cells analyzed. **(B)** Correlation of YFP versus RFP detection time for RFP-positive Vero cells (1 PFU per drop, blue stars; 10 PFU per drop, purple squares; 100 PFU per drop, black circle) (linear regression: $t_{RFP+} = 6.4 + 0.9 \times t_{YFP+}$, $P = 1.1 \times 10^{-7}$, $R^2 = 0.22$). **(C)** Representative images of Vero cells infected in drop on microgels. White circles outline the microgel. Scale bar, 50 µm.

single-cell transcriptomic studies of HSV-1 infection in epithelial cells (*2*) and neurons (*16*). Each study reported several hours of variation in the onset of viral gene expression despite synchronous inoculation. Further analyses observed that infected cells exhibit high cell-to-cell variability in late viral protein detection and abundance, suggesting that the progression of HSV-1 infection may be variable in single cells (*17*). These studies conclude that heterogeneity in HSV-1 infection is caused more by cell-to-cell variation in metabolic or immunological states within the population of susceptible and permissive cells.

Our results suggest that inoculating dose can also play a critical role in determining the productive outcome of infection. We observed that inoculating dose directly affects the kinetics of viral gene expression and the likelihood of productive replication. Our co-flow inoculation system enables precise manipulation of inoculating doses, mixed in drops with individual cells. We observed that YFP became detectable earlier in all cells infected with higher inoculating doses. All RFP-positive neurons were detectably YFP positive before 6 hpi, suggesting that early viral transcription is more likely to elicit productive viral replication. The dose dependence on viral gene expression and productive replication aligns with other work that observed dose-dependent HSV-1 replication in human foreskin fibroblasts (*40*). Similarly, the effects of lower inoculating dose leading to slower kinetics of expression and low rates of productive replication have been observed during HSV-1 infection of other nonneuronal cells (*33*, *40*). Notably, we were able to observe single-cell infection of neurons for longer observation periods. This extended observation window revealed a substantial population of "stalled" infections, where

YFP-positive cells fail to progress to RFP positivity. At lower inoculating doses (1 and 10 PFU per drop), we observe a large proportion (>93%) of cells stalling in their progression, while at 100 PFU per drop, a majority (>56%) of cells progress to RFP expression. We hypothesize that this nonlinear dependence on inoculating dose in progressing to RFP detection signifies an aborted or suppressed infection (*2*). However, further studies are required to understand the stage of viral replication at which progression stalls and the cellular factors that influence this outcome of infection.

To further understand the complexities of the microgel in-drop infection system, we investigated the effects of the microgel, the susceptible cell, and viral inoculum. We hypothesized that cells cultured within the microgel were inaccessible to infection, which is consistent with the minimal infection observed at 10 PFU per drop for Vero cells. Particle diffusion experiments demonstrate a lack of virion diffusion into the Matrigel. Therefore, cells cultured in microgel are limited in their spatial accessibility to HSV-1 infection. However, cells cultured on microgel were found to be accessible to HSV-1 and achieved a maximum of 95.2 ± 2.2% infection. The accessibility of cells to infection may partially explain why only a maximum of 78% of neurons express detectable YFP following our highest inoculating dose. The SCG neurons needed to be first encapsulated within the microgel, after which cell bodies and neurites could migrate to the gel surface. It is possible that some of the cells that did not express detectable YFP were inaccessible to infection. Alternatively, it is possible that these FP-negative cells were infected but represent a population of neurons that suppressed all viral gene expression.

While this system offers a powerful tool for investigating HSV-1 infection dynamics, there are limitations. In native tissue, neurons typically exist in microenvironments surrounded by other neurons and support cells such as glia, which may potentially influence cellular responses to infection. Isolated neurons lacking synaptic connectivity and glial support may exhibit distinct behaviors, potentially affecting the observed outcomes of HSV-1 infection. However, the substantial throughput and improved efficiency of this technique for single-neuron growth, infection, and analysis represent a notable advantage for assaying infection. Downstream single-cell analysis of infected cells via polymerase chain reaction (PCR) or sequencing promises to uncover cellular genes influencing the observed heterogeneity in HSV-1 infection. One caveat of our study is that, while the downstream recovery of neuronal soma is possible, retrieving intact neurons from the microgels for further processing poses challenges. The microgels provide the structural support needed to maintain fragile neurites. To overcome potential axotomy issues, techniques such as immunostaining and in situ hybridization allow for the single-cell evaluation of intact cells. In addition, this platform is adaptable for upstream interventions using small molecules, enabling the study of neuronal signaling and antiviral responses to infection. Moreover, a neuron-Vero coculture system could be used to investigate HSV-1 transmission. As with all methodologies, there are important points to consider and potentially refine with continued research and development. That said, the insights we have gained into heterogeneous outcomes of HSV-1 infection are sufficient to justify the continued exploration of individual cell culture and infection.

In conclusion, we demonstrate in-drop infection of single primary neurons cultured using microgels. The speed and scale of these microfluidic methods hold the potential for high-throughput culturing and assaying of single neurons. The microgels could also act as a scaffold for in-drop differentiation and manipulation of other primary cells (28, 29). While many approaches to droplet cell culture rely on suspension cells to study viral infection and replication (3, 21, 24), we observed an approximate 52% increase in infection when cells were cultured on microgels, compared to the same cells cultured in suspension. Last, our drop-based single-cell approach captures heterogeneous events within a population that would otherwise be missed by bulk culturing (3). In conclusion, the use of microgels for high-throughput single-cell culturing can provide a valuable tool for future research in neurobiology and virology studies, further enhancing our understanding of factors that affect viral replication dynamics.

MATERIALS AND METHODS
Vero cell culture
Vero cells purchased from the American Type Culture Collection (Manassas, VA) were maintained and subcultured in Dulbecco's modified Eagle's medium (DMEM) supplemented with 10% (v/v) fetal bovine serum (FBS) and 1% penicillin/streptomycin in 5% CO_2 at 37°C.

Mouse SCG neuron dissociation
Mouse SCGs were excised from embryos at 14 days after gestation from pregnant C57Bl/6 mice. The protocol for isolating SCGs is approved by the Institutional Animal Care and Use Committee at Montana State University (protocol no. 2022-52-IA). In brief, isolated SCGs were washed with Hanks' balanced saline solution (HBSS) and resuspended in trypsin (0.25 mg/ml; Gibco) in HBSS for dissociation

and incubated for 15 min in a 37°C water bath. Trypsinized SCGs were centrifuged and resuspended in trypsin inhibitor (1 mg/ml; Gibco) in HBSS and then incubated for 5 min in a 37°C water bath. Next, SCGs were centrifuged and resuspended in complete neurobasal [neurobasal media (Gibco), 1× B27 (Gibco), 2.5S nerve growth factor (60 ng/ml; MilliporeSigma), and 1% penicillin/streptomycin + glutamate (Gibco)] and dissociated by trituration using a 5-ml Pasteur pipette (41). Dissociated neurons were then cultured as described in complete neurobasal media.

Dual-reporter HSV-1
Dual-reporter HSV-1 was constructed, isolated, and characterized as previously described (30). Vero cells were used for viral stock production and plaque assay estimation of viral titers.

Microfluidic device fabrication
Negative master molds for the microfluidic devices were prepared using standard photolithography techniques (42). Negative master molds were made with Nano SU-8-100 photoresist (Microchem, Round Rock, TX, USA) on three silicon wafers (University Wafer Inc., Boston, MA, USA, University Wafer ID: 447). The microgel drop-maker and the suspension cell co-flow inoculating device were fabricated to be 100 μm tall. The co-flow microgel inoculating drop-maker and the DropSOAC (31) chambers were fabricated to be 150 μm tall. Devices were treated with (tridecafluoro-1,1,2,2-tetrahydrooctyl) trichlorosilane (1%, v/v) (Gelest) in fluorinated oil HFE 7500 (3M, Saint Paul, MN, USA) and left for solvent evaporation at 55°C.

Microgel production and cell encapsulation/seeding
Matrigel microgels were produced through drop-based microfluidics using previously established protocols (43). In brief, liquid Matrigel at 4°C and 1.5% (w/w) fluorosurfactant (008, RAN Biotechnologies, MA, USA) in HFE 7500 were loaded into luer lock syringes and injected into the 100-μm drop-maker using syringe pumps, which is designed to produce 100-μm microgels. The flow rates used were $Q_{Matrigel} = 100$ μl/hour and $Q_{HFE} = 900$ μl/hour. All equipment and reagents were refrigerated at 4°C to prevent premature gelation of the Matrigel. Drops were collected in microcentrifuge tubes and incubated at 37°C for 35 min to gel the drops. The resulting microgels were washed with equal volumes of $1H,1H,2H,2H$-perfluoro-octanal (PFO)–HFE 7500 (20%, v/v) and phosphate-buffered saline (PBS) to drops. The cleaned microgels were then collected in PBS.

In experiments where Vero cells or dissociated SCG neurons were encapsulated in microgels, cells were suspended in the liquid Matrigel at 1×10^6 cells/ml before drop making. After collecting the resulting microgels in PBS, they were placed in well plates with the appropriate growth medium. Vero cells were maintained in DMEM–10% FBS–1% penicillin/streptomycin in 5% CO_2 at 37°C for 4 hours before experimentation. SCG neurons were grown in complete neurobasal media at 37°C in a 5% CO_2 enriched atmosphere for 7 days before experimentation to allow maturation and neurite growth. Twenty-four hours after encapsulation, SCGs were supplemented with 1 μM cytosine-β-ᴅ arabinofuranoside (Sigma-Aldrich, C6645), a compound cytotoxic to mitotically active, non-neuronal cells. In experiments where Vero cells were seeded onto the microgels, empty microgels were mixed with 1×10^6 cells/1 ml of Microgel in a well plate. Cells were allowed to adhere for 4 hours before experimentation.

Immunofluorescence staining and imaging

After 7 days in culture, neurons grown in microgels were collected in microcentrifuge tubes and washed with PBS. Cells were fixed with 1% glutaraldehyde for 1 min and washed three times with PBS. Cells were blocked with 2% bovine serum albumin (BSA)/PBS at room temperature for 1 hour and washed three times with PBS. Cells were permeabilized with 0.1% Triton X-100/0.125% BSA/PBS and washed three times with 0.125% BSA/PBS. The primary antibody, anti–phosphorylated neurofilament H (NF-H) (BioLegend), was added at 5 µg/ml, incubated at room temperature overnight, and then washed three times in 0.125% BSA/PBS. The secondary antibody, goat anti-mouse immunoglobulin G (H+L), DyLight 550 (#84540, Thermo Fisher Scientific), and Hoechst 33342 solution (Thermo Fisher Scientific) were added at 5 and 20 µg/ml, respectively, for 1 hour at 37°C and then washed three times with 0.125% BSA/PBS. Cells and microgels were loaded onto glass slides and imaged on an epifluorescence microscope (Nikon Ti2). Cells were imaged in phase contrast/4′,6-diamidino-2-phenylindole (DAPI)/RFP.

In-drop infection procedures

Cells were infected in drops. To infect cells seeded onto or cultured in microgels, microgels were collected from well plates and pelleted by centrifuging the microgels at 200g for 1 min. The pelleted microgels were loaded into luer lock syringes. HSV-1 inoculum was diluted into the appropriate media. For Vero infections, HSV-1 stock was diluted in DMEM–10% FBS–1% penicillin/streptomycin. For SCG infections, HSV-1 stock was diluted in complete neurobasal media. HSV-1 was diluted at concentrations of 1.1×10^6, 1.1×10^7, and 1.1×10^8 PFU/ml, resulting in inoculating conditions of 1, 10, and 100 PFU per drop, respectively. The virus solutions and a 1.5% solution of RAN fluorosurfactant in HFE were loaded into individual luer lock syringes. The three syringes were loaded onto syringe pumps and injected into the appropriate inlet channels of the microfluidic co-flow microgel inoculation device, which is designed to produce 150-µm droplets. Flow rates were $Q_{HFE} = 2500$ µl/hour, and $Q_{Matrigel} = Q_{Virus} = 250$ µl/hour. Drops were collected into microcentrifuge tubes and either placed in an incubator at 37°C for end-point imaging or injected into DropSOAC chambers for time-lapse imaging.

To infect Vero cells suspended in media, Vero cells were removed from subculture using trypsin-EDTA and washed in PBS. Cells were suspended in DMEM–10% FBS–1% penicillin/streptomycin at 1×10^6 cells/ml and loaded into a luer lock syringe. HSV-1 was diluted into DMEM–10% FBS–1% penicillin/streptomycin at a concentration of 3.8×10^7 PFU/ml, resulting in an inoculating condition of 10 PFU per drop. The virus solution and a 1.5% solution of RAN fluorosurfactant in HFE were loaded into individual luer lock syringes. The three syringes were loaded onto syringe pumps and injected into the appropriate inlet channels of the co-flow suspension cell inoculating drop-maker. Flow rates were $Q_{HFE} = 2000$ µl/hour, and $Q_{Cells} = Q_{Virus} = 250$ µl/hour. Drops were collected into microcentrifuge tubes and placed in an incubator at 37°C for end-point imaging.

End-point imaging of inoculated cells

To visualize in-drop infection, drops were loaded into capillary tubes and imaged. Cells were imaged in phase contrast/fluorescein isothiocyanate (FITC)/tetramethyl rhodamine isothiocyanate (TRITC). To quantify the percentage of infected cells at 16 hpi, the drops containing infected cells were broken using 20% (v/v) PFO-HFE. Breaking the emulsion allowed for easier visualization and quantification of

cells. The broken supernatant containing infected cells was pipetted onto a polytetrafluoroethylene-printed microscope slide and imaged.

Time-lapse imaging of inoculated cells

To track the progression of FP detection in single cells, drops containing infected cells were loaded into DropSOAC devices with modified aluminum capsules (31). The capsules were placed in a microscope stage top incubation chamber (OKOlab) at 37°C. Images in phase contrast/YFP/RFP were taken every 15 min for 16 hours. Tile scans of each chamber were taken to capture as many cells as possible. Image acquisition began within 1 hour after inoculation.

Viability assay of cells in suspension

Vero cells were removed from triplicate subculture using trypsin-EDTA and washed in PBS. Cells were suspended in DMEM–10% FBS–1% penicillin/streptomycin at 1×10^6 cells/ml and loaded into a luer lock syringe. A 1.5% solution of RAN fluorosurfactant in HFE was loaded into another luer lock syringe. Both syringes were then loaded onto syringe pumps and introduced into the corresponding inlet channels of a drop-maker. Flow rates were $Q_{HFE} = 2000$ µl/hour and $Q_{Cells} = 1000$ µl/hour. Drops were collected into microcentrifuge tubes and placed in an incubator at 37°C for end-point imaging. Samples taken from replicate Vero cultures at the time of emulsification were immediately stained, as described below, and imaged for a 0-hour viability assessment. After 16 hours of incubation, Vero cells suspended in drops were released from the emulsion by adding PFO-HFE 7500 (20%, v/v) to the drops. Released cells were immediately stained and imaged for a 16-hour viability assessment. Stained cells were incubated for 20 min at 37°C in DMEM supplemented with CellTracker Green CMFDA (10 µM working concentration, Invitrogen, C7025) and PI (7.5 µM working concentration, MilliporeSigma, 537060). Stained cells were washed with PBS and plated in media for imaging. Cells were imaged for CellTracker fluorescence using a green fluorescent protein filter set and PI fluorescence using an RFP filter set with equal exposure and excitation power parameters between time points and image fields.

HSV-1 diffusion with Matrigel experiments

To evaluate HSV-1 virion diffusion through Matrigel, a time-lapse imaging series of virions interacting with the Matrigel interface was performed via inverted laser scanning confocal microscopy (iCLSM) (Stellaris DMI8, Leica). Matrigel (20 µl) was pipetted onto a 35-mm glass-bottom dish (MatTek) and gelled at 37°C, forming a hemisphere of solid gel on the glass surface. PBS was added to the glass-bottom dish to submerge the Matrigel. The PBS and Matrigel-containing dish were placed on the microscope stage, and a time-lapse imaging series (XYT) was initiated, with the focal point centered on the Matrigel-PBS interface. At $t = 0$ min, 1×10^7 PFU of mRFP-VP26–tagged virions or 1×10^8 of yellow-green fluorescent–tagged nanoparticles (160 nm, FluoSpheres Carboxylate-Modified Microspheres, catalog no. F8811, Thermo Fisher Scientific) were added to the dish. Images were acquired at 63 times every 10 min for 90 min in two channels: a transmitted light channel (bright field) and a fluorescence channel (mRFP and FITC).

Statistical analysis
Percentage of YFP-positive cells

To quantify the percentage of YFP-positive cells, end-point images were analyzed using Fiji ImageJ (44). Cells were found in bright field.

The background intensity of the YFP channel was subtracted from the image, and the percentage of YFP-positive cells was quantified. Experiments were repeated in triplicate. Cell counts for Vero cells embedded in microgels ranged from 79 to 280 cells per replicate, for Vero cells grown on microgels from 165 to 390 cells per replicate, for Vero cells in suspension from 228 to 456 cells per replicate, and for SCG neurons from 84 to 209 cells per replicate. Multiple comparison tests and one-way ANOVAs were performed in MATLAB.

The timing of YFP and RFP detection
To quantify the timing of YFP and RFP detection, time-lapse images were analyzed using Fiji ImageJ (*44*). Cells were difficult to identify in bright field, so cells were identified by finding YFP-positive cells at 16 hpi. Once located, a 30-μm-diameter circular region of interest (ROI) was drawn around each individual cell. The maximum pixel intensity in YFP and RFP for the ROI was then measured for each time frame. The frame 1 maximum pixel intensity of each ROI was subtracted from the subsequent frames for that ROI. The noise threshold was found to be 50 arbitrary units (a.u.) for YFP and 75 a.u. for RFP. The timing of YFP and RFP detection was defined as the first time frame the YFP and RFP pixel intensities in each ROI were greater than the noise threshold for two consecutive frames. For SCG time-lapse studies, experiments were repeated three to four times with a total of 174 cells analyzed. For Vero time-lapse studies, experiments were repeated three times with a total of 669 cells analyzed. One-way ANOVAs and linear regressions were performed in MATLAB.

Supplementary Materials
This PDF file includes:
Fig. S1
Legend for movie S1

Other Supplementary Material for this manuscript includes the following:
Movie S1

REFERENCES AND NOTES
1. C. Simpson, S. S. Lee, C.-S. Lee, Y. Yamauchi, Microfluidics: An untapped resource in viral diagnostics and viral cell biology. *Curr. Clin. Microbiol. Rep.* **5**, 245–251 (2018).
2. N. Drayman, P. Patel, L. Vistain, S. Tay, HSV-1 single-cell analysis reveals the activation of anti-viral and developmental programs in distinct sub-populations. *eLife* **8**, e46339 (2019).
3. W. Liu, H. He, S.-Y. Zheng, Microfluidics in single-cell virology: Technologies and applications. *Trends Biotechnol.* **38**, 1360–1372 (2020).
4. A. B. Russell, E. Elshina, J. R. Kowalsky, A. J. W. Te Velthuis, J. D. Bloom, Single-cell virus sequencing of influenza infections that trigger innate immunity. *J. Virol.* **93**, (2019).
5. A. B. Russell, C. Trapnell, J. D. Bloom, Extreme heterogeneity of influenza virus infection in single cells. *eLife* **7**, e32303 (2018).
6. S. Y. Kupke, L.-H. Ly, S. T. Börno, A. Ruff, B. Timmermann, M. Vingron, S. Haas, U. Reichl, Single-cell analysis uncovers a vast diversity in intracellular viral defective interfering RNA content affecting the large cell-to-cell heterogeneity in influenza A virus replication. *Viruses* **12**, 71 (2020).
7. F. S. Heldt, S. Y. Kupke, S. Dorl, U. Reichl, T. Frensing, Single-cell analysis and stochastic modelling unveil large cell-to-cell variability in influenza A virus infection. *Nat. Commun.* **6**, 8938 (2015).
8. Y. Zhu, A. Yongky, J. Yin, Growth of an RNA virus in single cells reveals a broad fitness distribution. *Virology* **385**, 39–46 (2009).
9. F. Guo, S. Li, M. U. Caglar, Z. Mao, W. Liu, A. Woodman, J. J. Arnold, C. O. Wilke, T. J. Huang, C. E. Cameron, Single-cell virology: On-chip investigation of viral infection dynamics. *Cell Rep.* **21**, 1692–1704 (2017).
10. A. Timm, J. Yin, Kinetics of virus production from single cells. *Virology* **424**, 11–17 (2012).
11. J. Sun, J. C. Vera, J. Drnevich, Y. T. Lin, R. Ke, C. B. Brooke, Single cell heterogeneity in influenza A virus gene expression shapes the innate antiviral response to infection. *PLOS Pathog.* **16**, e1008671 (2020).
12. A. C. Wilson, Impact of cultured neuron models on α-herpesvirus latency research. *Viruses* **14**, 1209 (2022).
13. M. E. Marcocci, G. Napoletani, V. Protto, O. Kolesova, R. Piacentini, D. D. Li Puma, P. Lomonte, C. Grassi, A. T. Palamara, G. De Chiara, Herpes simplex virus-1 in the brain: The dark side of a sneaky infection. *Trends Microbiol.* **28**, 808–820 (2020).
14. J. R. Heath, J. A. Dembowski, Fashionably late: Temporal regulation of HSV-1 late gene transcription. *PLOS Pathog.* **18**, e1010536 (2022).
15. B. Roizman, G. Zhou, The 3 facets of regulation of herpes simplex virus gene expression: A critical inquiry. *Virology* **479–480**, 562–567 (2015).
16. H.-L. Hu, K. P. Srinivas, S. Wang, M. V. Chao, T. Lionnet, I. Mohr, A. C. Wilson, D. P. Depledge, T. T. Huang, Single-cell transcriptomics identifies Gadd45b as a regulator of herpesvirus-reactivating neurons. *EMBO Rep.* **23**, e53543 (2022).
17. M. K. Pietilä, J. J. Bachmann, J. Ravantti, L. Pelkmans, C. Fraefel, Cellular state landscape and herpes simplex virus type 1 infection progression are connected. *Nat. Commun.* **14**, 4515 (2023).
18. D. García Alonso, M. Yu, H. Qu, L. Ma, F. Shen, Advances in microfluidics-based technologies for single cell culture. *Adv. Biosyst.* **3**, e1900003 (2019).
19. A. B. Theberge, F. Courtois, Y. Schaerli, M. Fischlechner, C. Abell, F. Hollfelder, W. T. S. Huck, Microdroplets in microfluidics: An evolving platform for discoveries in chemistry and biology. *Angew. Chem. Int. Ed. Engl.* **49**, 5846–5868 (2010).
20. E. K. Loveday, G. K. Zath, D. A. Bikos, Z. J. Jay, C. B. Chang, Screening of additive formulations enables off-chip drop reverse transcription quantitative polymerase chain reaction of single influenza A virus genomes. *Anal. Chem.* **93**, 4365–4373 (2021).
21. E. K. Loveday, H. S. Sanchez, M. M. Thomas, C. B. Chang, Single-cell infection of influenza A virus using drop-based microfluidics. *Microbiol. Spectr.* **10**, e0099322 (2022).
22. A. Rotem, A. W. R. Serohijos, C. B. Chang, J. T. Wolfe, A. E. Fischer, T. S. Mehoke, H. Zhang, Y. Tao, W. Lloyd Ung, J.-M. Choi, J. V. Rodrigues, A. O. Kolawole, S. A. Koehler, S. Wu, P. M. Thielen, N. Cui, P. A. Demirev, N. S. Giacobbi, T. R. Julian, K. Schwab, J. S. Lin, T. J. Smith, J. M. Pipas, C. E. Wobus, A. B. Feldman, D. A. Weitz, E. I. Shakhnovich, Evolution on the biophysical fitness landscape of an RNA virus. *Mol. Biol. Evol.* **35**, 2390–2400 (2018).
23. Y. Tao, A. Rotem, H. Zhang, S. K. Cockrell, S. A. Koehler, C. B. Chang, L. W. Ung, P. G. Cantalupo, Y. Ren, J. S. Lin, A. B. Feldman, C. E. Wobus, J. M. Pipas, D. A. Weitz, Artifact-free quantification and sequencing of rare recombinant viruses by using drop-based microfluidics. *Chembiochem* **16**, 2167–2171 (2015).
24. H. Zhang, S. K. Cockrell, A. O. Kolawole, A. Rotem, A. W. R. Serohijos, C. B. Chang, Y. Tao, T. S. Mehoke, Y. Han, J. S. Lin, N. S. Giacobbi, A. B. Feldman, E. Shakhnovich, D. A. Weitz, C. E. Wobus, J. M. Pipas, Isolation and analysis of rare norovirus recombinants from coinfected mice using drop-based microfluidics. *J. Virol.* **89**, 7722–7734 (2015).
25. A. E. Fischer, S. K. Wu, J. B. G. Proescher, A. Rotem, C. B. Chang, H. Zhang, Y. Tao, T. S. Mehoke, P. M. Thielen, A. O. Kolawole, T. J. Smith, C. E. Wobus, D. A. Weitz, J. S. Lin, A. B. Feldman, J. T. Wolfe, A high-throughput drop microfluidic system for virus culture and analysis. *J. Virol. Methods* **213**, 111–117 (2015).
26. Y. Tao, A. Rotem, H. Zhang, C. B. Chang, A. Basu, A. O. Kolawole, S. A. Koehler, Y. Ren, J. S. Lin, J. M. Pipas, A. B. Feldman, C. E. Wobus, D. A. Weitz, Rapid, targeted and culture-free viral infectivity assay in drop-based microfluidics. *Lab Chip* **15**, 3934–3940 (2015).
27. M. Frega, 3D neuronal networks: State of the art, in *Neuronal Network Dynamics in 2D and 3D In Vitro Neuroengineered Systems*, M. Frega, Ed. (Springer International Publishing, 2016), pp. 45–57.
28. A. S. Caldwell, B. A. Aguado, K. S. Anseth, Designing microgels for cell culture and controlled assembly of tissue microenvironments. *Adv. Funct. Mater.* **30**, 1907670 (2020).
29. Y. Xu, H. Zhu, A. Denduluri, Y. Ou, N. A. Erkamp, R. Qi, Y. Shen, T. P. J. Knowles, Recent advances in microgels: From biomolecules to functionality. *Small* **18**, e2200180 (2022).
30. L. F. Domanico, G. P. Dunn, O. Kobiler, M. P. Taylor, A dual-fluorescent recombinant for live observation of herpes simplex-type 1 infection outcomes. bioRxiv 2023.06.07.544108 [Preprint] (2023). https://doi.org/10.1101/2023.06.07.544108.
31. S. L. Pratt, G. K. Zath, T. Akiyama, K. S. Williamson, M. J. Franklin, C. B. Chang, DropSOAC: Stabilizing microfluidic drops for time-lapse quantification of single-cell bacterial physiology. *Front. Microbiol.* **10**, 2112 (2019).
32. C. H. J. Schmitz, A. C. Rowat, S. Köster, D. A. Weitz, Dropspots: A picoliter array in a microfluidic device. *Lab Chip* **9**, 44–49 (2009).
33. E. M. Cohen, O. Kobiler, Gene expression correlates with the number of herpes viral genomes initiating infection in single cells. *PLOS Pathog.* **12**, e1006082 (2016).
34. J. Witten, K. Ribbeck, The particle in the spider's web: Transport through biological hydrogels. *Nanoscale* **9**, 8080–8095 (2017).
35. O. Lieleg, K. Ribbeck, Biological hydrogels as selective diffusion barriers. *Trends Cell Biol.* **21**, 543–551 (2011).
36. N. Broguiere, L. Isenmann, C. Hirt, T. Ringel, S. Placzek, E. Cavalli, F. Ringnalda, L. Villiger, R. Züllig, R. Lehmann, G. Rogler, M. H. Heim, J. Schüler, M. Zenobi-Wong, G. Schwank, Growth of epithelial organoids in a defined hydrogel. *Adv. Mater.* **30**, e1801621 (2018).
37. S. Maday, A. E. Twelvetrees, A. J. Moughamian, E. L. F. Holzbaur, Axonal transport: Cargo-specific mechanisms of motility and regulation. *Neuron* **84**, 292–309 (2014).

38. W. M. Tierney, I. A. Vicino, S. Y. Sun, W. Chiu, E. A. Engel, M. P. Taylor, I. B. Hogue, Methods and applications of campenot trichamber neuronal cultures for the study of neuroinvasive viruses. *Methods Mol. Biol.* **2431**, 181–206 (2022).

39. J. Gordon, S. Amini, M. K. White, General overview of neuronal cell culture, in *Neuronal Cell Culture: Methods and Protocols*, S. Amini, M. K. White, Eds. (Humana Press, 2013), pp. 1–8.

40. K. M. Scherer, J. D. Manton, T. K. Soh, L. Mascheroni, V. Connor, C. M. Crump, C. F. Kaminski, A fluorescent reporter system enables spatiotemporal analysis of host cell modification during herpes simplex virus-1 replication. *J. Biol. Chem.* **296**, 100236 (2021).

41. T. H. Ch'ng, E. A. Flood, L. W. Enquist, Culturing primary and transformed neuronal cells for studying pseudorabies virus infection. *Methods Mol. Biol.* **292**, 299–316 (2005).

42. J. P. Fredrikson, P. P. Brahmachary, A. E. Erdoğan, Z. K. Archambault, J. N. Wilking, R. K. June, C. B. Chang, Metabolomic profiling and mechanotransduction of single chondrocytes encapsulated in alginate microgels. *Cell* **11**, 900 (2022).

43. Z. Mahdieh, M. D. Cherne, J. P. Fredrikson, B. Sidar, H. S. Sanchez, C. B. Chang, D. Bimczok, J. N. Wilking, Granular Matrigel: Restructuring a trusted extracellular matrix material for improved permeability. *Biomed. Mater.* **17**, 045020 (2022).

44. C. T. Rueden, J. Schindelin, M. C. Hiner, B. E. DeZonia, A. E. Walter, E. T. Arena, K. W. Eliceiri, ImageJ2: ImageJ for the next generation of scientific image data. *BMC Bioinformatics* **18**, 529 (2017).